WO$_x$/ZrO$_x$ functionalised periodic mesoporous organosilicas as water-tolerant catalysts for carboxylic acid esterification[†]

Vannia C. dos Santos-Durndell[a,‡], Lee J. Durndell,(ⓘ 0000-0002-2391-5233)[a,‡,*], Mark A. Isaacs,(ⓘ 0000-0002-0335-4272)(J-9870-2014)[b,c], Adam F. Lee[d,*] and Karen Wilson,(ⓘ 0000-0003-4873-708X)(A-1061-2009)[d,*]

[a]School of Geography, Earth and Environmental Sciences, Plymouth University, Plymouth, PL4 8AA, UK, lee.durndell@plymouth.ac.uk, +44 (0)1752 584763

[b]Department of Chemistry, University College London, London, WC1E 6BT, UK

[c]HarwellXPS, Research Complex at Harwell, Rutherford Appleton Laboratory, Didcot, Oxfordshire, OX11 0DE, UK

[d]Centre for Advanced Materials and Industrial Chemistry (CAMIC), RMIT University, Melbourne, VIC, 3000, Australia, adamfraserlee@gmail.com, karen.wilson2@rmit.edu.au

[‡]These authors contributed equally to this work.

Funding Information

Table of Contents Entry

Kicking out water: Oeptimising the interaction between support hydrophobicity and surface acid sites in WO$_x$/ZrO$_x$/PMO catalysts unlocks an efficient route for the upgrading of low-quality waste bio-oil feedstocks to biodiesel. Imparting increasing catalyst water tolerance, through phenyl group incorporation, promotes the rapid esterification of free fatty acids to their fatty acid methyl esters, while suppressing undesired ester hydrolysis.

Abstract

Catalyst hydrophobicity is an oft-neglected property despite its significance in aqueous phase reactions and those wherein water is a by-product, such as condensation and esterification. Here we synthesise WO$_x$/ZrO$_x$ impregnated periodic mesoporous organosilicas (PMOs) of varying organic framework content, through the stepwise

substitution of bis(triethoxysilyl)benzene (BTSB) for tetraethyl orthosilicate (TEOS), followed by tungsten and zirconium co-grafting. Incorporation of phenyl groups into the framework of mesoporous SBA-15 silica imparts surface hydrophobicity and tunes the solid acidity, while preserving the textural properties of the parent silica. The resulting $WO_x/ZrO_x/PMO$ catalysts exhibit excellent turnover frequencies (TOFs) for the esterification of $C_3–C_{16}$ carboxylic acids in methanol at 60 °C, with TOFs inversely proportional to fatty acid chain length. The superior activity and stability (water tolerance up to 50 mol%) of $WO_x/ZrO_x/PMO$ *versus* $WO_x/ZrO_x/SBA$-15 is attributed to the displacement of water from in-pore active sites, mitigating the reverse ester hydrolysis reaction. Such hydrophobic, solid acid catalysts are anticipated to find widespread application in aqueous phase synthesis, particularly of biorefinery output streams.

Introduction

The sustainable production of fuels and value-added chemicals from waste resources is of critical importance in the fight against climate change and the transition to a greener, circular economy.[1–3] As such, the invention of efficient new processes to reduce society's reliance on fossil fuels is a grand challenge in the 21st century.[4–6] The catalytic conversion of waste lignocellulosic and oleaginous biomass to biofuels are two such routes garnering increasing attention to address such challenges.[7,8]

Biodiesel typically comprises fatty acid methyl esters (FAME) with $C_{10–25}$ chain length and is produced by the base-catalysed transesterification of triglycerides (TAG) with methanol using Na or K methoxide. Common viable feedstocks for biodiesel include non-food derived sources from jatropha or castor oil, or a range of waste palm, soy, sunflower, or rapeseed cooking oils,[9] of which have high free fatty acid (FFA) contents. While base-catalysed transesterification routes are efficient, unfortunately, they are unsuitable for direct use with high FFA-containing waste oils, leading to catalyst neutralisation and saponification, and thus acid-catalysed esterification to remove FFA is a major component of this process (Scheme 1).

Scheme 1

General mechanism for carboxylic acid esterification.
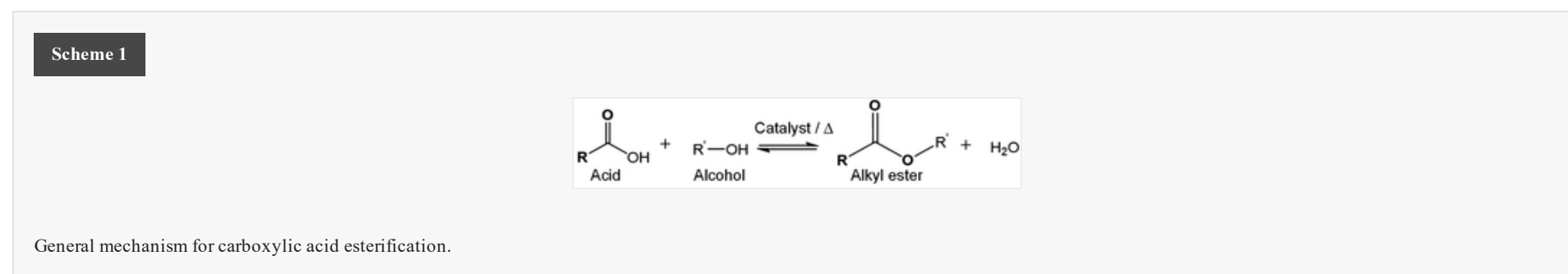
The use of homogeneous catalysts is however undesirable as extensive aqueous quenching, neutralisation and separation steps are required after each step, and to meet strict guidelines relating to residual alkali concentration in biofuels (<5 ppm).[10,11] Estimates suggest 0.2–3 L of alkali-contaminated wastewater is produced for every litre of biodiesel produced,[12] which requires energy intensive remediation treatment that hinders overall economic viability and increases the carbon footprint of biodiesel production.[13]

The use of heterogeneous acid catalysts offers facile separation and purification of biodiesel, increasing process efficiency by negating the need for aqueous quenches and enabling opportunities to operate continuous processes. Solid acidity may be integral to a material, *e.g.* aluminosilicates, or introduced into a material that has otherwise desirable properties. For the latter, acid functionalisation may occur *via* covalent bonding of *e.g.* a molecular acid to a surface (*e.g.* propylsulfonic acid); the incorporation of an acid function to a framework (*e.g.* of a metal cation); or through composite formation. Examples of such solids acid catalysts for FFA esterification include zeolites[14] and heteropolyacids,[15,16] organically functionalised silicas,[17,18] and tungstated[19] and sulphated ZrO_2.[20,21] Tungstated zirconia (WO_x/ZrO_2) is a particularly attractive (composite) solid acid catalyst for FFA esterification owing to its excellent stability towards leaching and strong acidity.[22,23] Unfortunately commercially available microporous solid acid catalysts exhibit several operational shortcomings, and their catalytic activity is often significantly lower than homogeneous counterparts.[24,25] Notably, their microporous nature is incompatible with bulky FFAs leading to poor in-pore mass-transport,[26,27] and the hydrophilic nature of metal oxide-based solid acids (*e.g.* zeolites) make them highly sensitive to poisoning by either adventitious or reactively formed water in the reactant feed. The use of acid-functionalised polymer resins such as sulfonated Amberlyst-15 beads is often explored for esterification, however the reliance of resin gel swelling to expose acid sites, and microporosity of cross-linked macroreticular beads leads to diffusion limitation,[28,29] and their practical application is further hampered by the poor stability of acid sites towards water poisoning.[30,31] The presence of water, often a major component in low-grade feedstocks, is also problematic as it can promote undesired ester hydrolysis pathways and leaching of solid acid sites.[32] Esterification is an equilibrium-limited reaction, in which the accumulation of reactively-formed water by-product drives ester hydrolysis back to the carboxylic acid reactant.[33] High conversions are therefore only achievable through either process engineering (*e.g.* reactive distillation or pervaporation membranes) or catalyst engineering to remove water from the active site. The latter necessitates the development of mesoporous catalysts with excellent active site accessibility to minimise diffusion limitation, and tailored surface hydrophobicity[34] to retard water chemisorption and improve catalyst productivity and lifetime.[35,36] Such mechanistic dependencies are not unique to esterification reactions, elevated surface hydrophobicity has been shown to promote methane adsorption pathways (and subsequent conversion) over palladium/ceria-praseodymia catalysts for direct methane oxidation.[37] Increased hydrocarbon affinity of hydrophobic Ag/Al_2O_3 catalysts was also beneficial in mitigating site-blocking deactivation phenomena in the catalytic reduction of NO_x to N_2.[38] Controlling surface polarity and hydrophobicity is therefore a powerful route to improve the water tolerance of metal oxides, which can be achieved in mesoporous silicas either through organic group functionalisation[17,39] or using periodic mesoporous organosilicas.[40]

Tunable hydrophobicity in hybrid organic-silica materials can result from the direct incorporation of organic groups in the walls or as pendant groups on the surface of the templated silica.[41–43] However, for pendant groups, loading achievable by simple grafting routes are limited by surface tethering sites and competes with sites required for grafting of active sites,[17] while loss of structural order can result from 'one-pot' approaches where organosilanes are co-condensed with tetraethyl orthosilicate (TEOS) at high loading.[44] Periodic mesoporous organosilicas (PMOs) are an interesting class of material which incorporate organic groups directly into the walls of mesostructured silicas using organo-bridged siloxanes,[45–48] and exhibit high specific surface areas >1000 m^2 g^{-1} and pore diameters 1.5–10 nm.[49–51] Incorporating bridging organics in the pore walls of PMOs enables retention of surface silanols necessary for active site tethering, critical for use in a range of applications including catalysis,[52] water treatment,[53] enzyme immobilisation,[49] and gas separation.[54] Brønsted acid functionalised PMOs are generally based on sulfonic acid derivatised materials, with applications including phenol condensation with acetone to bisphenol A,[52] cellobiose hydrolysis to glucose,[55] fructose dehydration to 5-HMF,[56] Diels–Alder reactions,[57] transesterification[58,59] and esterification.[60] The benefits of hydrophobicity on sulfonic acid derivatised ethyl[61,62] and phenyl[63] bridged PMO materials have been reported for esterification with activity surpassing that of commercial resins. Our previous work on sulfonic acid functionalised PMOs revealed that 1,4-bis-(triethoxysilyl)benzene (BTSB) co-condensation with TEOS affords a higher turnover frequency (TOF) for FFA esterification than 1.2-bis(triethoxysilyl)ethane (BTSE) analogues.[64] Nevertheless, organic functions such as tethered alkyl/aryl sulfonic acids are less thermally stable than their inorganic counterparts, and more difficult to characterise by IR, XPS or NMR when attached to PMOs, due to the presence of carbon in both the acid function (*e.g.* propyl or phenyl linkers) and the organosilica support. Although
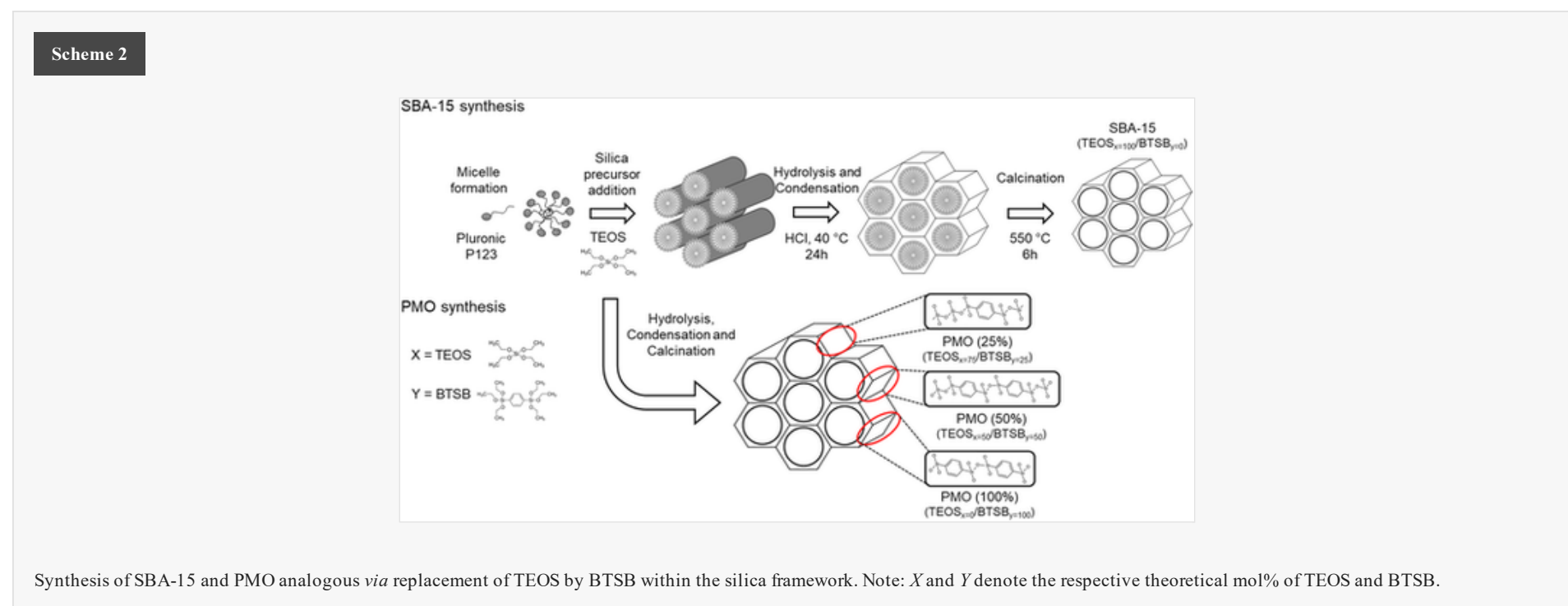
various organic moieties have been incorporated into silicas to create PMOs,[34] 1.2-bis(triethoxysilyl)ethane (BTSE) and bis(triethoxysilyl)benzene (BTSB) are the most studied for catalysis as they offer a more homogeneous carbon distribution and improved surface crystallinity and thermal stability.[45,46]

Alternative SO_4/ZrO_2-PMO materials synthesised by co-condensation of 1,4-bis-(triethoxysilyl)benzene (BTESB) with $Zr(OBu)_4$ and $(NH_4)_2SO_4$ (ref. [65]) (or post-functionalised with chlorosulfonic acid[66]) have also been reported which offer Brønsted acidity for plant oil transesterification (or Brønsted and Lewis acidity for the cascade synthesis of ethyl levulinate from glucose) with excellent water tolerance. Despite their strong acidity, sulfated zirconia is prone to SO_4^{2-} leaching in polar reaction mixtures at high temperature. Metals such as Zr can be directly incorporated into PMO frameworks by one-pot syntheses using, e.g. zirconocene dichloride, to form pure Lewis acidic Zr-PMOs that are highly stable catalysts for biodiesel synthesis from crude feedstocks containing 20 wt% water.[40] However, incorporation of framework Zr must be limited to avoid loss of structural order of the PMO framework, with maximum acid site densities $\sim$0.2 mmol g^{-1}. To improve surface Zr loadings while retaining structure, post-modification, thin film deposition would be desirable,[67] with the added benefit of enabling further functionalisation with more stable e.g. WO_x species to generate Brønsted acidity.

Herein, we report on the synthesis and application of a water-tolerant solid acid catalyst for FFA esterification, prepared from a bis(triethoxysilyl) benzene functionalised PMO post-modified with a thin film of WO_x/ZrO_x. The effect of BTSB content on catalyst physicochemical and resultant catalytic performance for the esterification of a range of C_3–C_{16} carboxylic acids is discussed. Use of a hydrophobic support promotes the expulsion of reactively-formed water from inorganic solid acid catalysts; water that would otherwise drive undesired hydrolysis of ester products, produced from fatty acid esterification. Selection of a periodic mesoporous organosilica as the hydrophobic support facilitates close proximity of the (easily accessible) active sites and aromatic components of the support, essential to fabricating water tolerant catalysts able to produce FAME from low quality feedstocks e.g. waste cooking oil.

Results and discussion

Three PMO supports were synthesised with varying concentrations of phenyl-bridged siloxane units through partial/complete substitution of the tetraethyl orthosilicate (TEOS) precursor used in a conventional SBA-15 synthesis[68] by bis(triethoxysilyl) benzene (BTSB). The resulting materials are designated PMO(x%) wherein x is the theoretical mol% (25, 50 or 100) of organosilica species contributed by BTSB versus TEOS in the synthesis. A conventional SBA-15 support was also prepared for comparison. The synthetic route is illustrated in Scheme 2. Acid functionality was introduced to these four supports by adapting a literature method[40] wherein tungsten chloride and zirconium(IV) isopropoxide were used as respective tungsten and zirconium precursors for co-grafting in hexane and subsequent hydrolysis to their oxides. Physicochemical properties of parent and WO_x/ZrO_x impregnated SBA-15 and PMO supports were determined by XRD, XRF, XPS, HRTEM, CHNS, pyridine diffuse reflectance infrared Fourier transform spectroscopy (DRIFTS), NH_3 pulse chemisorption, solid state $^1H/^{29}Si$ magic-angle spinning (MAS)-NMR and N_2 porosimetry.

Scheme 2

Synthesis of SBA-15 and PMO analogous via replacement of TEOS by BTSB within the silica framework. Note: X and Y denote the respective theoretical mol% of TEOS and BTSB.

All parent and WO_x/ZrO_x functionalised supports exhibited relatively large Brunauer–Emmett–Teller (BET) surface areas (spanning 578–1000 m^2 g^{-1}) (Table 1, Fig. S1 and S2†). The PMO materials exhibited type IV adsorption isotherms with H1 hysteresis loops,[69] characteristic of the parent SBA-15 which possesses hexagonal close-packed arrangements of cylindrical mesopores of $p6mm$ symmetry. Nitrogen isotherms exhibited a shift to lower relative pressure with increasing BTSB content in the synthesis, as previously reported for metal-functionalised PMO analogues[40,70,71] and ascribed to a reduction in mesopore diameter and volume and increased microporosity. Applying the BJH method to the desorption branch of N_2 isotherms can introduce artefacts for smaller (<8 nm) and ink-bottle/slit-shaped mesopores in silicas, and in porous carbons, erroneously resulting in multiple peaks in the pore size distribution (Fig. S1 and S2†). Non-local density functional theory (NLDFT) models are more accurate for such materials, and we therefore applied a NLDFT model (designed for nitrogen adsorption over mesoporous silicas such as SBA-15 based on a cylindrical pore model) implemented within the Quantachrome NovaWin software. The resulting pore size distributions reveal progressive narrowing of mesopore channels (Table 1, Fig. S1 and S2†), in general agreement with corresponding HRTEM measurements (Table S1†). Micropore analysis by the t-plot method confirmed that BTSB incorporation in the synthesis was accompanied by an increase in micropore surface area for the parent PMOs (Table 1). Melero et al.[72] proposed that such textural changes arise from enhanced micelle penetration into the organosilicon pore walls during assembly of the templated silica superstructure due to the affinity of BTSB and silica precursors.[73] Nitrogen porosimetry and low angle XRD evidenced that textural and crystalline properties of the parent PMOs were largely retained following functionalisation by WO_x/ZrO_x, although with a significant drop in surface area and pore volume. Low-angle XRD patterns exhibited peaks at 2θ = 0.9, 1.5 and 1.7°, corresponding to the (100), (110) and (200) reflections of the hexagonal close-packed mesopores, for all BTSB concentrations (Fig. S3 and S4†), however the d_{100} spacings increased with % BTSB due in part to the aforementioned micelle effects which result in smaller mesopores, and a concomitant increase in pore wall thickness (Table 1).[74]

Table 1

Physicochemical properties of parent and WO_x/ZrO_x functionalised supports

Sample	Surface area ^{a} (m^2 g^{-1})	Pore diameter^b (nm)	Total pore volume^b (cm^3 g^{-1})	Unit cell parameter^c (nm)	Wall thickness^d (nm)	Micropore area^e (m^2 g^{-1})	Bulk W content^f (wt%)	Bulk Zr content^f (wt%)	Bulk C content^g (wt%)	Surface C content^h (wt%)

SBA-15	874	8.2	1.4	10.59	2.5	99	—	—	—	—
PMO(25%)	879	7.0	1.1	10.59	3.6	257	—	—	—	—
PMO(50%)	888	6.8	1.0	10.60	3.8	385	—	—	—	—
PMO(100%)	1000	6.6	0.9	10.61	4.1	450	—	—	—	—
WO_x/ZrO_x/SBA-15	632	6.8	0.9	10.59	3.8	90	2.1	39.4	2.4	1.2
WO_x/ZrO_x/PMO(25%)	574	6.6	0.7	10.59	4.0	210	1.5	18.7	6.2	5.4
WO_x/ZrO_x/PMO(50%)	598	6.1	0.5	10.60	4.5	148	2.0	18.8	11.7	9.6
WO_x/ZrO_x/PMO(100%)	684	5.9	0.6	10.59	4.7	143	2.0	26.3	27.7	17.9

Table Footnotes

[a]BET.

[b]NLDFT.

[c]Determined from $a_0 = (2d_{100})/\sqrt{3}$.

[d]Determined from a_0 – pore diameter.

[e]t-plot method.

[f]Bulk W/Zr content from XRF.

[g]Bulk C content from CHN.

[h]Surface C content from XPS.

Elemental analysis confirmed a systematic increase in the carbon content (from 2 to 30 wt%) with increasing BTSB incorporation (Table 1), supported by an increase in thermogravimetric mass loss from 300 to 800 °C, due to pyrolysis of the organic component (Fig. S5[†]). A similar W loading for all WO_x/ZrO_x grafted materials although the W : Zr mass ratio showed significant variation. Negligible residual Cl was detected by ICP-MS (Table S2[†]) consistent with XPS (Fig. S6[†]). Comparison of bulk and surface compositions by CHN and XPS indicates a uniform spatial distribution of carbon (BTSB) without any surface enrichment, as expected for BTSB incorporation into the silica framework. No ZrO_2 or WO_x crystalline phases were apparent from wide-angle XRD (Fig. S4[†]) indicating the deposition of dispersed (<2 nm) Zr and W oxide species on the SBA-15 and PMO supports. Elemental mapping by EDX evidenced a uniform distribution of W and Zr throughout the mesopore network and across the external surface (Fig. S7[†]), consistent with similar bulk and surface W and Zr contents observed by XRF/ICP-MS (Tables 1 and S2[†]) and XPS (Table S2[†]), respectively. As the transition metals were introduced by post-modification of the SBA-15 and PMO supports they cannot occupy framework sites, unlike previous one-pot syntheses.[40] Corresponding HRTEM imaging (Fig. S8–S11[†]) confirmed the presence of ordered arrays of parallel hexagonal close-packed mesopores. EDX line scans perpendicular to mesopore channels in WO_x/ZrO_x/SBA-15 (Fig. S8c[†]) and WO_x/ZrO_x/PMO(100%) (Fig. S11c[†]) revealed periodic variations in the W and Zr concentrations, with periodicities similar to the respective pore diameters and hence indicative of metal coated pore walls. Single pulse ^{29}Si and ^{1}H magic-angle spinning (MAS)-NMR was used to quantify organosilica incorporation into SBA-15 framework (Fig. 1a and b).


Fig. 1
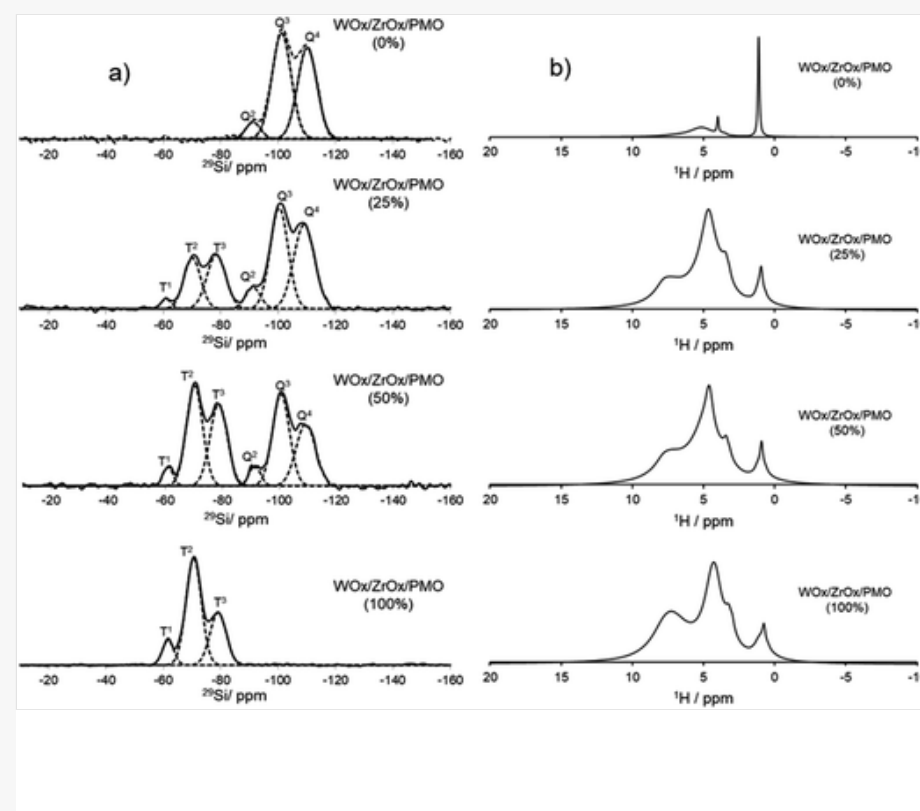
(a) ^{29}Si NMR spectra, and (b) ^{1}H NMR spectra of WO_x/ZrO_x impregnated SBA-15 and PMOs. Note: Q^4 = Si(OSi)$_4$; Q^3 = (HO)Si(OSi)$_3$; Q^2 = (HO)$_2$Si(OSi)$_2$; T^3 = RSi(OSi)$_3$; T^2 = R(HO)Si–(OSi)$_2$; T^1 = R(HO)$_2$Si(OSi).

According to Glaser *et al.*[75] the chemical shift of ^{29}Si nuclei are sensitive to their local environment: T species (δ = −60 to −80 ppm) are characteristic of organosilica species (and hence BTSB), while Q species (δ = −90 to −110 ppm) are associated with TEOS. Our ^{29}Si MAS-NMR spectra confirm a transition from Q to T species with increasing BTSB (decreasing TEOS) in the synthesis. Such observations are consistent with previous reports for PMOs[40,75,76] wherein, under acidic conditions, the initial formation of mesostructured silicas from organosilica precursors in the presence of alkenyloxide block copolymers generates a high concentration of surface hydroxyls which react to form siloxane bridges upon surfactant removal. Complementary ^{1}H MAS NMR spectra of WO_x/ZrO_x-impregnated SBA-15 and PMO materials all exhibit three peaks with common chemical shifts of approximately 1.1, 3.5 and 4.8 ppm. That at 1.1 ppm is assigned to isolated silanol surface functionalities (Si–OH) expected to impart weak acidic or neutral character. The peaks at 3.5 (sharp) and 4.8 ppm (broad) are assigned to weakly bound silanol groups and/or physisorbed water, respectively.[77] An additional peak at 7.3 ppm is observed for all BTSB-substituted PMOs (absent from the WO_x/ZrO_x-impregnated SBA-15), whose intensity steadily increases with increasing BTSB incorporation. This peak is ascribed to strongly acidic surface hydroxyls at the surface of tungstated zirconia, arising from coordination of W–OH with unsaturated Lewis acidic Zr^{4+} sites to form Brønsted acidic bridging W–OH–Zr hydroxyls.[78] Raman analyses confirmed the presence of BTSB in all PMOs, evidenced by phenyl bands at 590, 634, 781, 1107 and 1205 cm^{-1} for all WO_x/ZrO_x/PMOs (Fig. 2 and S12[†]).[79] The relative peak widths of the 590 cm^{-1} and 634 cm^{-1} bands differ

significantly between free and silica incorporated BTSB, the broader low wavenumber band being characteristic of a PMO.[80] An additional band at 936 cm^{-1} is indicative of polytungstate species,[81] consistent with the W 4f$_{7/2}$ XP binding energies of WO$_x$/ZrO$_x$/SBA-15 and WO$_x$/ZrO$_x$/PMOs (Fig. S13†) which evidence W(VI) in polytungstate clusters (the corresponding Zr 4p$_{1/2}$ binding energy of ~31.9 eV being consistent with Zr(IV) in ZrO$_2$).[19]


Fig. 2
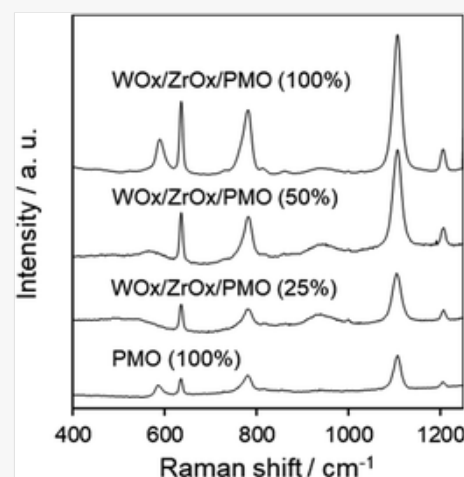
Raman spectra of WO$_x$/ZrO$_x$ impregnated PMOs. Spectrum of 100% PMO without WO$_x$/ZrO$_x$ provided as reference.

Surface acidity was subsequently investigated *via* the temperature-programmed decomposition of propylamine (Hofmann rearrangement) to propene,[82] NH$_3$ pulse chemisorption and DRIFTS of chemisorbed pyridine (Fig. 3b). Total acid site loadings were inversely proportional to the BTSB content (Table S2† and Fig. 3a), falling from ~1 mmol g^{-1} for WO$_x$/ZrO$_x$/SBA-15 to 0.5 mmol g^{-1} for WO$_x$/ZrO$_x$/PMO(100%). This trend is attributed to preferential adsorption of W and Zr precursors over hydrophilic silica patches. Although all catalysts contain a similar W and Zr content (Table 1), confinement of WO$_x$/ZrO$_x$ moieties to increasingly smaller surface footprints is expected to drive a transition from isolated monotungstate and polytungstate clusters over SBA-15 to two-dimensional polytungstates or small 3D nanoparticles over PMO(100%),[19,83] thereby reducing the number of acid sites. Note: these acid loadings far exceed those achievable by the introduction of Zr into a PMO framework (0.06–0.23 mmol g^{-1}).[40] The decrease in acid loading with increasing BTSB addition was accompanied xby a small increase in acid strength (Fig. S14†), indicated by a shift in the desorption peak maximum of reactively-formed propene from 419.8 °C to 401.4 °C,[84] attributed to the Brønsted acidic bridging W–OH–Zr hydroxyls apparent from ^{1}H NMR (Fig. 1b). Brønsted/Lewis acid character was also a weak function of BTSB content, with SBA-15 exhibiting similar intensity IR bands from chemisorbed pyridine at 1610 cm^{-1}, 1575 cm^{-1} and 1445 cm^{-1} (attributed to molecular pyridine bound to Lewis acids of WO$_x$/ZrO$_x$,[85–87] Fig. 3b), and at 1640 cm^{-1} and 1540 cm^{-1} (attributed to pyridinium ions bound to Brønsted acid sites[88]). The band at 1597 cm^{-1} is ascribed to pyridine physisorbed to silanols.[89] The band at 1489 cm^{-1} is attributed to pyridine bound to both Brønsted and Lewis acid sites. Organosilica incorporation into the silica framework induced a progressive increase in Brønsted acidity, evidenced by progressive weakening of the 1610 cm^{-1} band. This may be attributed to a systematic change in surface silanol coverage (*i.e.* surface polarity) with increasing BTSB substitution, as indicated by ^{1}H/^{29}Si MAS NMR measurements (Fig. 1).


Fig. 3
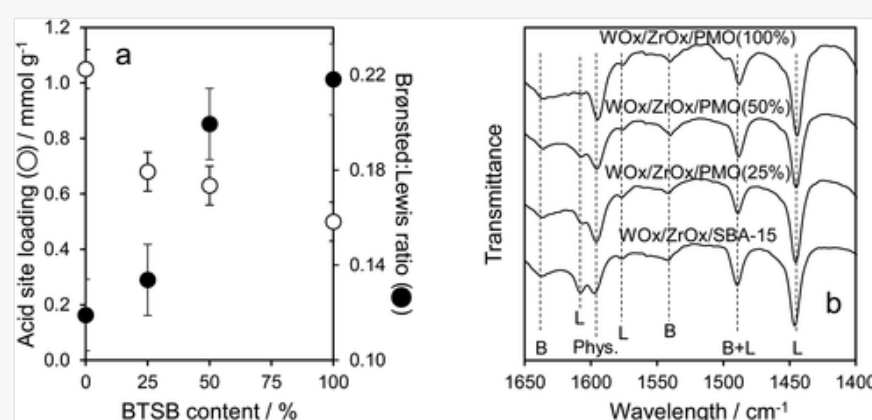
(a) Dependence of total acid site loading (from NH$_3$ chemisorption) and Brønsted : Lewis acidity (from FTIR of chemisorbed pyridine), and (b) *in vacuo* DRIFT spectra of pyridine on WO$_x$/ZrO$_x$ as a function of BTSB content.

Carboxylic acid esterification

The esterification of C$_3$–C$_{16}$ carboxylic acids with methanol over WO$_x$/ZrO$_x$ impregnated PMOs was subsequently investigated (Fig. 4 and S15–S18†), with the proposed mechanism illustrated in Fig. S19.† Esterification is a spontaneous reaction, but very slow at 60 °C with <2% conversion over 6 h observed in the absence of catalyst (Fig. S20†). All WO$_x$/ZrO$_x$ impregnated PMOs were active for esterification, with the highest conversions observed for the two highest BTSB contents in the synthesis; 6 h conversions decreased with chain length from ~90% for propanoic acid to ~50% for palmitic acid. Turnover frequencies (TOFs) per acid site were proportional to BTSB content in the synthesis (Fig. S18†), and hence Brønsted solid acid character (Fig. 4a), and inversely proportional to acid chain length (Fig. 4b) attributed to diffusion limitations in combination with polar and steric effects for the bulkier reactants.[21,90–92] The greatest impact of BTSB addition to the synthesis was apparent for the WO$_x$/ZrO$_x$/PMO(100%) for which TOFs increased between 200 and 300% compared with WO$_x$/ZrO$_x$/SBA-15 for all carboxylic acids. However, there was no correlation between the magnitude of TOF enhancement for esterification and acid chain length, suggesting that BTSB did not influence the rate of molecular transport through the catalyst mesopore network. Introduction of phenyl groups into the silica framework also had no effect on either W or Zr surface chemical environments (Fig. S13†); no shifts were observed in the core-level binding energies of either metal, or in the W : Zr surface atomic ratios, between different samples. The most likely explanation for BTSB-promoted esterification is therefore the displacement of reactively-formed water (by-product) away from Brønsted acid active sites within the hydrophobic pore network, thereby shifting the reaction equilibrium in favour of the ester product.[33] A similar phenomenon is invoked for acetic acid esterification with methanol and butanol respectively catalysed by octyl co-functionalised propylsulfonic SBA-15 (ref. 17) and MCM-41 (ref. 93) mesoporous silicas, wherein improved activity was attributed to surface hydrophobicity and resulting mitigation of undesired ester hydrolysis.

Fig. 4
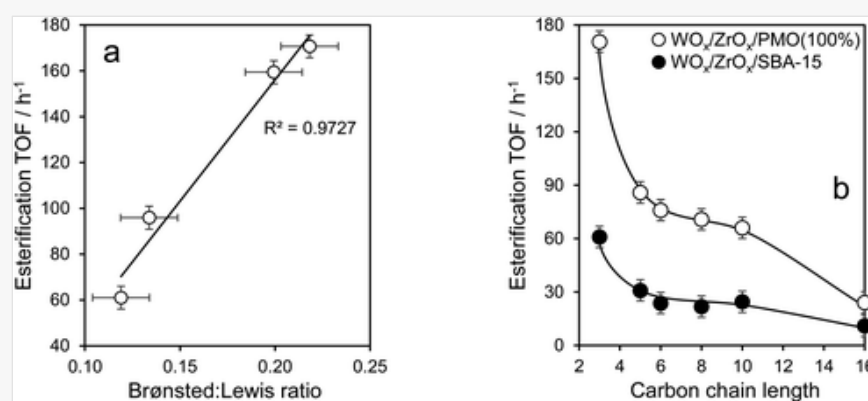
(a) Relationship between Brønsted : Lewis ratio and TOF for propanoic acid esterification and (b) turnover frequencies for C_3–C_{16} carboxylic acid esterification with methanol over $WO_x/ZrO_x/SBA$-15 and $WO_x/ZrO_x/PMO(100\%)$. Reaction conditions: 60 °C, 12.5 mL MeOH, 30 : 1 molar ratio MeOH : acid, 0.025 g (C_3–C_8 acids) and 0.050 g (C_{10}–C_{16} acids) catalyst, 800 rpm.

To further examine the influence of BTSB on catalyst hydrophobicity and suppression of ester hydrolysis, the water sensitivity of $WO_x/ZrO_x/SBA$-15 and $WO_x/ZrO_x/PMOs$ was compared for propanoic acid esterification (Fig. 5a). The addition of 5 mmol water (0.5 molar equivalents) to propanoic acid lowered TOFs for all catalysts, however, this simply reflects a shift in the equilibrium towards reactants, and hence should not be considered deactivation (catalyst performance is recoverable by removing the water or increasing the methanol and acid concentration).[94] The magnitude of this TOF suppression is inversely proportional to the organic content of the silica framework. Catalysts derived from <50% BTSB exhibited a 40% decrease in TOF while those with higher loadings experienced only a 20–30% decrease. The most hydrophobic $WO_x/ZrO_x/PMO(100\%)$ catalyst retained 80% of its original activity, consistent with literature PMO catalysts in water–sensitive reactions.[52,63,95,96]

Fig. 5
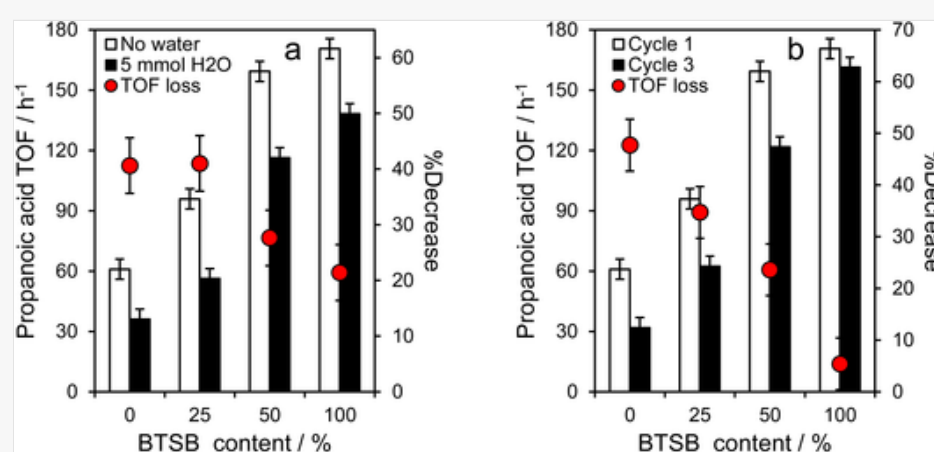
Impact of (a) 5 mmol water addition, and (b) recycling on propanoic acid esterification with methanol over WO_x/ZrO_x impregnated SBA-15 and PMOs. Reaction conditions: 60 °C, 12.5 mL MeOH, 30 : 1 molar ratio MeOH : acid, 0.025 g catalyst, 800 rpm.

Benchmarking against related literature catalysts under similar reaction conditions (temperature and alcohol : acid ratios) for a range of carboxylic acids (Fig. S21†) reveals that $WO_x/ZrO_x/PMO(100\%)$ outperforms Amberlyst-15, unsupported WO_x/ZrO_x, WS_2, propylsulfonic acid and even superacidic SO_4/ZrO_2 (except for hexanoic acid). Catalyst stability was also studied through recycle experiments (Fig. 5b). Spent catalysts were recovered by filtration, washed three times with methanol, and subsequently re-used for two further esterification reaction cycles. A fresh reaction mixture was employed for all reactions. The $WO_x/ZrO_x/SBA$-15 catalyst exhibited significant deactivation (a 50% loss in TOF) after three reaction cycles. Introduction of BTSB into the mesoporous silica synthesis improved catalyst resistance to deactivation, with the magnitude of this stabilisation proportional to the extent of initial BTSB content; negligible deactivation was observed for $WO_x/ZrO_x/PMO(100\%)$. Analysis of catalysts post-reaction suggests that catalyst deactivation was not due to *in situ* sintering of W or Zr phases (Fig. S22†), with neither W nor Zr crystalline phases observed for $WO_x/ZrO_x/SBA$-15 or $WO_x/ZrO_x/PMO(100\%)$. There was also no evidence of metal leaching by XRF analysis of the catalysts (Table S3†). However, ultimate analysis reveals the magnitude of the activity loss of our catalysts was proportional to the amount of surface carbon accumulated post-reaction (Fig. S22†), which we attribute to the formation of metal carboxylates.

Conclusions

Functionalisation of phenyl-bridged, periodic mesoporous organosilicas (PMOs) by tungstated zirconia (WO_x/ZrO_x) yields hydrophobic solid acid catalysts active for the esterification of C_3–C_{16} free fatty acids with methanol. The introduction of between 25 and 100 mol% organic linkers into the framework of SBA-15 systematically reduced total pore volumes and mesopore diameters, accompanied by a significant increase in microporosity. Surface area and porosity were further reduced following wet impregnation by highly dispersed WO_x/ZrO_x. Although the total acid site loading of WO_x/ZrO_x functionalised (organo)silicas decreased with organic framework content (from 1 mmol g^{-1} for SBA-15 to 0.5 mmol g^{-1} for $WO_x/ZrO_x/PMO(100\%)$), this was offset by a concomitant rise in Brønsted acidity and esterification turnover frequencies for all fatty acids. The latter observation is attributed to the expulsion of reactively-formed water from the mesoporous network and concomitant suppression of undesired ester hydrolysis. Esterification activity was inversely proportional to fatty acid size, likely reflecting limited in-pore diffusion and steric effects for longer-chain acids. Increasing the hydrophobic character of the silica framework (*via* phenyl incorporation) significantly improved water tolerance for propanoic acid esterification, even in the presence of 0.5 mol equivalents relative to the carboxylic acid. Hydrophobising the SBA-15 support also improved catalyst stability by reducing the accumulation of strongly-adsorbed organic species which may be responsible for blocking of active sites. Extending the synthesis of such solid acid PMOs to macroporous analogues would enhance their application to the respective esterification and transesterification of long-chain FFAs and TAGs present in non-edible and waste bio-oils, and hence facilitate the one-pot production of biodiesel.

Author contributions

Vannia C. dos Santos-Durndell: conceptualization, methodology, data curation, formal analysis, writing − original draft, writing − review and editing. Lee J. Durndell: conceptualization, resources, methodology, data curation, formal analysis, investigation, writing − original draft, writing − review and editing. Mark A. Isaacs: data curation, formal analysis. Karen Wilson: conceptualization, resources, writing − review and editing. Adam F. Lee: conceptualization, resources, writing − review and editing.

Conflicts of interest

There are no known competing financial or personal interests.

Acknowledgements

References

ⓘ References can be edited in the panel that appears to the right when you click on a reference.

1 A. M. Oliveira, R. R. Beswick and Y. Yan, *Curr. Opin. Chem. Eng.*, 2021, **33**, 100701.

2 T. Raj, K. Chandrasekhar, R. Banu, J.-J. Yoon, G. Kumar and S.-H. Kim, *Fuel*, 2021, **303**, 121333.

3 S. Basumatary, B. Nath, B. Das, P. Kalita and B. Basumatary, *Fuel*, 2021, **286**, 119357.

4 A. Jain, S. Sarsaiya, M. Kumar Awasthi, R. Singh, R. Rajput, U. C. Mishra, J. Chen and J. Shi, *Fuel*, 2022, **307**, 121859.

5 L. R. Lynd, *Nat. Biotechnol.*, 2017, **35**, 912–915.

6 G. W. Huber, S. Iborra and A. Corma, *Chem. Rev.*, 2006, **106**, 4044–4098.

7 J. G. W. Siqueira, C. Rodrigues, L. P. d. S. Vandenberghe, A. L. Woiciechowski and C. R. Soccol, *Biomass Bioenergy*, 2020, **132**, 105419.

8 C. Wang, X. Zhang, Q. Liu, Q. Zhang, L. Chen and L. Ma, *Fuel Process. Technol.*, 2020, **208**, 106485.

9 N. Asikin-Mijan, D. Derawi, N. Salih, J. Salimon, G. A. Alsultan, M. S. Mastuli and M. X. Y. Ravindran, in Innovations in Thermochemical Technologies for Biofuel Processing, ed. S. Nanda and D.-V. Vo, Elsevier, 2022, 197–219, 10.1016/B978-0-323-85586-0.00002-0

10 A. Avinash, D. Subramaniam and A. Murugesan, *Renewable Sustainable Energy Rev.*, 2014, **29**, 517–527.

11 G. Berndes, J. Hansson, A. Egeskog and F. Johnsson, *Biomass Bioenergy*, 2010, **34**, 227–236.

12 V. B. Veljković, O. S. Stamenković and M. B. Tasić, *Renewable Sustainable Energy Rev.*, 2014, **32**, 40–60.

13 I. M. Rizwanul Fattah, H. C. Ong, T. M. I. Mahlia, M. Mofijur, A. S. Silitonga, S. M. A. Rahman and A. Ahmad, *Front. Energy Res.*, 2020, **8**, 101.

14 A. Osatiashtiani, B. Puértolas, C. C. S. Oliveira, J. C. Manayil, B. Barbero, M. Isaacs, C. Michailof, E. Heracleous, J. Pérez-Ramírez, A. F. Lee and K. Wilson, *Biomass Convers. Biorefin.*, 2017, **7**, 331–342.

15 A. Alsalme, E. F. Kozhevnikova and I. V. Kozhevnikov, *Appl. Catal., A*, 2008, **349**, 170–176.

16 Y. Leng, J. Wang, D. Zhu, Y. Wu and P. Zhao, *J. Mol. Catal. A: Chem.*, 2009, **313**, 1–6.

17 J. C. Manayil, V. C. dos Santos, F. C. Jentoft, M. Granollers Mesa, A. F. Lee and K. Wilson, *ChemCatChem*, 2017, **9**, 2231–2238.

18 J. Dhainaut, J.-P. Dacquin, A. F. Lee and K. Wilson, *Green Chem.*, 2010, **12**, 296–303.

19 V. C. dos Santos, K. Wilson, A. F. Lee and S. Nakagaki, *Appl. Catal., B*, 2015, **162**, 75–84.

20 X.-R. Chen, Y.-H. Ju and C.-Y. Mou, *J. Phys. Chem. C*, 2007, **111**, 18731–18737.

21 A. Osatiashtiani, L. J. Durndell, J. C. Manayil, A. F. Lee and K. Wilson, *Green Chem.*, 2016, **18**, 5529–5535.

22 D. E. López, K. Suwannakarn, D. A. Bruce and J. G. Goodwin, *J. Catal.*, 2007, **247**, 43–50.

23 D. E. López, J. G. Goodwin, D. A. Bruce and E. Lotero, *Appl. Catal., A*, 2005, **295**, 97–105.

24 V. Mandari and S. K. Devarai, *BioEnergy Res.*, 2022, **15**, 935–961.

25 K. Ngaosuwan, X. Mo, J. G. Goodwin and P. Praserthdam, *Appl. Catal., A*, 2010, **380**, 81–86.

26 E. M. Björk, M. P. Militello, L. H. Tamborini, R. Coneo Rodriguez, G. A. Planes, D. F. Acevedo, M. S. Moreno, M. Odén and C. A. Barbero, *Appl. Catal., A*, 2017, **533**, 49–58.

27 M. A. Isaacs, N. Robinson, B. Barbero, L. J. Durndell, J. C. Manayil, C. M. A. Parlett, C. D'Agostino, K. Wilson and A. F. Lee, *J. Mater. Chem. A*, 2019, **7**, 11814–11825.

28 E. Lotero, Y. Liu, D. E. Lopez, K. Suwannakarn, D. A. Bruce and J. G. Goodwin, *Ind. Eng. Chem. Res.*, 2005, **44**, 5353–5363.

29 C. Pirez, J.-M. Caderon, J.-P. Dacquin, A. F. Lee and K. Wilson, *ACS Catal.*, 2012, **2**, 1607–1614.

30 J.-Y. Park, Z.-M. Wang, D.-K. Kim and J.-S. Lee, *Renewable Energy*, 2010, **35**, 614–618.

31 N. Boz, N. Degirmenbasi and D. M. Kalyon, *Appl. Catal., B*, 2015, **165**, 723–730.

32 E. Minami and S. Saka, *Fuel*, 2006, **85**, 2479–2483.

33 Z. Khan, F. Javed, Z. Shamair, A. Hafeez, T. Fazal, A. Aslam, W. B. Zimmerman and F. Rehman, *J. Ind. Eng. Chem.*, 2021, **103**, 80–101.

34 J. C. Manayil, A. F. Lee and K. Wilson, *Molecules*, 2019, **24**, 239.

35 S. N. Gebremariam and J. M. Marchetti, *Energy Convers. Manage.*, 2018, **168**, 74–84.

36 M. A. Hanif, S. Nisar, M. N. Akhtar, N. Nisar and N. Rashid, *Int. J. Energy Res.*, 2018, **42**, 2070–2083.

37 S. Ballauri, E. Sartoretti, M. Hu, C. D'Agostino, Z. Ge, L. Wu, C. Novara, F. Giorgis, M. Piumetti, D. Fino, N. Russo and S. Bensaid, *Appl. Catal., B*, 2023, **320**, 121898.

38 K. Ralphs, C. D'Agostino, R. Burch, S. Chansai, L. F. Gladden, C. Hardacre, S. L. James, J. Mitchell and S. F. R. Taylor, *Catal. Sci. Technol.*, 2014, **4**, 531–539.

39 J. A. Melero, L. F. Bautista, G. Morales, J. Iglesias and D. Briones, *Energy Fuels*, 2009, **23**, 539–547.

40 R. Sánchez-Vázquez, C. Pirez, J. Iglesias, K. Wilson, A. F. Lee and J. A. Melero, *ChemCatChem*, 2013, **5**, 994–1001.

41 F. Hoffmann, M. Cornelius, J. Morell and M. Fröba, *Angew. Chem., Int. Ed.*, 2006, **45**, 3216–3251.

42 W. Whitnall, T. Asefa and G. A. Ozin, *Adv. Funct. Mater.*, 2005, **15**, 1696–1702.

43 Y. Xia, W. Wang and R. Mokaya, *J. Am. Chem. Soc.*, 2005, **127**, 790–798.

44 I. K. Mbaraka and B. H. Shanks, *J. Catal.*, 2005, **229**, 365–373.

45 S. Inagaki, S. Guan, T. Ohsuna and O. Terasaki, *Nature*, 2002, **416**, 304–307.

46 M. P. Kapoor, S. Inagaki, S. Ikeda, K. Kakiuchi, M. Suda and T. Shimada, *J. Am. Chem. Soc.*, 2005, **127**, 8174–8178.

47 B. Hatton, K. Landskron, W. Whitnall, D. Perovic and G. A. Ozin, *Acc. Chem. Res.*, 2005, **38**, 305–312.

48 P. Van Der Voort, D. Esquivel, E. De Canck, F. Goethals, I. Van Driessche and F. J. Romero-Salguero, *Chem. Soc. Rev.*, 2013, **42**, 3913–3955.

49 V. Gascón, I. Díaz, R. M. Blanco and C. Márquez-Álvarez, *RSC Adv.*, 2014, **4**, 34356–34368.

50 Q. Yang, J. Liu, J. Yang, L. Zhang, Z. Feng, J. Zhang and C. Li, *Microporous Mesoporous Mater.*, 2005, **77**, 257–264.

51 B. Schäfgen, O. D. Malter, E. Kaigarula, A. Schüßler, S. Ernst and W. R. Thiel, *Microporous Mesoporous Mater.*, 2017, **251**, 122–128.

52 Q. Yang, J. Liu, J. Yang, M. P. Kapoor, S. Inagaki and C. Li, *J. Catal.*, 2004, **228**, 265–272.

53 H. Zou, R. Wang, Z. Shi, J. Dai, Z. Zhang and S. Qiu, *J. Mater. Chem. A*, 2016, **4**, 4145–4154.

54 L. Wu, Z. Yu, Y. Ye, Y. Yang, H. Zeng, J. Huang, Y. Huang, Z. Zhang and S. Xiang, *J. Solid State Chem.*, 2018, **264**, 113–118.

55 J. Sun, X. Liu, X. Zhu, H. Wang, S. Rostamnia and J. Han, *Catalysts*, 2017, 7, 5, 127.

56 W. N. P. van der Graaff, K. G. Olvera, E. A. Pidko and E. J. M. Hensen, *J. Mol. Catal. A: Chem.*, 2014, **388–389**, 81–89.

57 K. Nakajima, I. Tomita, M. Hara, S. Hayashi, K. Domen and J. N. Kondo, *Catal. Today*, 2006, **116**, 151–156.

58 B. Karimi, H. M. Mirzaei and A. Mobaraki, *Catal. Sci. Technol.*, 2012, **2**, 828–834.

59 C. Pirez, M. T. Reche, A. F. Lee, J. C. Manayil, V. C. dos-Santos and K. Wilson, *Catal. Lett.*, 2015, **145**, 1483–1490.

60 S. An, D. Song, B. Lu, X. Yang and Y.-H. Guo, *Chem.–Eur. J.*, 2015, **21**, 10786–10798.

61 J. Liu, Q. Yang, M. P. Kapoor, N. Setoyama, S. Inagaki, J. Yang and L. Zhang, *J. Phys. Chem. B*, 2005, **109**, 12250–12256.

62 M. I. López, D. Esquivel, C. Jiménez-Sanchidrián, F. J. Romero-Salguero and P. Van Der Voort, *J. Catal.*, 2015, **326**, 139–148.

63 Q. Yang, M. P. Kapoor, S. Inagaki, N. Shirokura, J. N. Kondo and K. Domen, *J. Mol. Catal. A: Chem.*, 2005, **230**, 85–89.

64 C. Pirez, A. F. Lee, C. Jones and K. Wilson, *Catal. Today*, 2014, **234**, 167–173.

65 W. Li, F. Ma, F. Su, L. Ma, S. Zhang and Y. Guo, *ChemSusChem*, 2011, **4**, 744–756.

66 D. Song, Q. Zhang, Y. Sun, P. Zhang, Y.-H. Guo and J.-L. Hu, *ChemCatChem*, 2018, **10**, 4953–4965.

67 G. Morales, A. Osatiashtiani, B. Hernández, J. Iglesias, J. A. Melero, M. Paniagua, D. Robert Brown, M. Granollers, A. F. Lee and K. Wilson, *Chem. Commun.*, 2014, **50**, 11742–11745.

68 D. Zhao, J. Sun, Q. Li and G. D. Stucky, *Chem. Mater.*, 2000, **12**, 275–279.

69 K. S. W. Sing, *Pure Appl. Chem.*, 1985, **57**, 603–619.

70 J. T. A. Jones, C. D. Wood, C. Dickinson and Y. Z. Khimyak, *Chem. Mater.*, 2008, **20**, 3385–3397.

71 A. Styskalik, I. Kordoghli, C. Poleunis, A. Delcorte, C. Aprile, L. Fusaro and D. P. Debecker, *Microporous Mesoporous Mater.*, 2020, **297**, 110028.

72 J. A. Melero, J. Iglesias, J. M. Arsuaga, J. Sainz-Pardo, P. de Frutos and S. Blazquez, *J. Mater. Chem.*, 2007, **17**, 377–385.

73 M. Impéror-Clerc, P. Davidson and A. Davidson, *J. Am. Chem. Soc.*, 2000, **122**, 11925–11933.

74 H. I. Meléndez-Ortiz, L. A. García-Cerda, Y. Olivares-Maldonado, G. Castruita, J. A. Mercado-Silva and Y. A. Perera-Mercado, *Ceram. Int.*, 2012, **38**, 6353–6358.

75 R. H. Glaser, G. L. Wilkes and C. E. Bronnimann, *J. Non-Cryst. Solids*, 1989, **113**, 73–87.

76 S.-Y. Wu, H.-S. Hsueh and M. H. Huang, *Chem. Mater.*, 2007, **19**, 5986–5990.

77 R. Siegel, E. Domingues, R. De Sousa, F. Jérôme, C. M. Morais, N. Bion, P. Ferreira and L. Mafra, *J. Mater. Chem.*, 2012, **22**, 7412–7419.

78 J. Xu, A. Zheng, J. Yang, Y. Su, J. Wang, D. Zeng, M. Zhang, C. Ye and F. Deng, *J. Phys. Chem. B*, 2006, **110**, 10662–10671.

79 E. I. Ross-Medgaarden, W. V. Knowles, T. Kim, M. S. Wong, W. Zhou, C. J. Kiely and I. E. Wachs, *J. Catal.*, 2008, **256**, 108–125.

80 J. Morell, M. Güngerich, G. Wolter, J. Jiao, M. Hunger, P. J. Klar and M. Fröba, *J. Mater. Chem.*, 2006, **16**, 2809–2818.

81 Y. Peng, W. Si, X. Li, J. Chen, J. Li, J. Crittenden and J. Hao, *Environ. Sci. Technol.*, 2016, **50**, 9576–9582.

82 E. J. M. Hensen, D. G. Poduval, V. Degirmenci, D. A. J. M. Ligthart, W. Chen, F. Maugé, M. S. Rigutto and J. A. R. V. Veen, *J. Phys. Chem. C*, 2012, **116**, 21416–21429.

83 D. G. Barton, M. Shtein, R. D. Wilson, S. L. Soled and E. Iglesia, *J. Phys. Chem. B*, 1999, **103**, 630–640.

84 A. G. Palkhiwala and R. J. Gorte, *Catal. Lett.*, 1999, **57**, 19–23.

85 R. A. Boyse and E. I. Ko, *J. Catal.*, 1997, **171**, 191–207.

86 C.-Y. Wang, O. Kwon, R. J. Gorte and J. M. Vohs, *Microporous Mesoporous Mater.*, 2022, **335**, 111821.

87 M. Tamura, K.-i. Shimizu and A. Satsuma, *Appl. Catal., A*, 2012, **433–434**, 135–145.

88 G. Sunita, B. M. Devassy, A. Vinu, D. P. Sawant, V. V. Balasubramanian and S. B. Halligudi, *Catal. Commun.*, 2008, **9**, 696–702.

89 A. Ramírez, B. L. Lopez and L. Sierra, *J. Phys. Chem. B*, 2003, **107**, 9275–9280.

90 Y. Liu, E. Lotero and J. G. Goodwin, *J. Catal.*, 2006, **243**, 221–228.

91 J. L. Fiorio, A. H. Braga, C. L. B. Guedes and L. M. Rossi, *ACS Sustainable Chem. Eng.*, 2019, **7**, 15874–15883.

92 J. Lilja, D. Y. Murzin, T. Salmi, J. Aumo, P. Mäki-Arvela and M. Sundell, *J. Mol. Catal. A: Chem.*, 2002, **182–183**, 555–563.

93 J.-P. Dacquin, H. E. Cross, D. R. Brown, T. Düren, J. J. Williams, A. F. Lee and K. Wilson, *Green Chem.*, 2010, **12**, 1383–1391.

94 A. A. Kiss, A. C. Dimian and G. Rothenberg, *Adv. Synth. Catal.*, 2006, **348**, 75–81.

95 J. Liu, J. Yang, C. Li and Q. Yang, *J. Porous Mater.*, 2009, **16**, 273–281.

96 S. O. Ganiyu, C. Bispo, N. Bion, P. Ferreira and I. Batonneau-Gener, *Microporous Mesoporous Mater.*, 2014, **200**, 117–123.

Footnotes

Queries and Answers

Q1

Query: Have all of the author names been spelled and formatted correctly? Names will be indexed and cited as shown on the proof, so these must be correct. No late corrections can be made.

Answer: Yes

Q2

Query: The Graphical Abstract text currently exceeds the space available for the published version. Please trim the text so that it is shorter than 250 characters (including spaces).

Answer: Corrected and additional text removed

Q3

Query: Have all of the funders of your work been fully and accurately acknowledged?

Answer: Yes

Q4

Query: Ref. 13: Please provide the page (or article) number(s).

Answer: Page number updated

Q5

Query: Ref. 55: Please provide the page (or article) number(s).

Answer: Reference updated

Query: Have all of the funders of your work been fully and accurately acknowledged?

Answer: Yes

Query: Ref. 13: Please provide the page (or article) number(s).

Answer: Page number updated

Query: Ref. 55: Please provide the page (or article) number(s).